Characterization of the Eyjafjallajökull volcanic event over the Iberian Peninsula by LIDAR remote sensing and ground level data collection

M. A. Revuelta[1], M. Sastre[1], A. J. Fernández[1], L. Martin[2], R. García[2], F. J. Gomez-Moreno[1], B. Artiñano[1], M. Pujadas[1] & F. Molero[1]

[1] Grupo de Contaminación Atmosférica, CIEMAT, Avda. Complutense, 22. 28040 Madrid, Spain

[2] Agencia Estatal de Meteorología. Leonardo Prieto Castro, 8. 28040 Madrid, Spain

Abstract:

In April and May 2010 the eruption of the Eyjafjallajökull volcano disrupted air traffic across Europe. The vast economic impact of this event has stirred interest on accurate plume dispersion estimation and detailed ash characterization, in order to establish a more precise threshold for safe aircraft operation. In this work we study the physical and chemical properties of volcanogenic aerosol detected at ground level at several locations over the Iberian Peninsula, nearly 3000 Km away from the Icelandic volcano. Between 4 and 13 May, volcanogenic aerosol was detected at ground level, identified by an increase in sulfur dioxide, particle mass concentrations, sulfate in precipitation and particulate sulfate concentration, at most EMEP/GAW/CAMP stations as well as at the CIEMAT site (for the sulfate concentration in PM). At the CIEMAT site, the synergic use of Raman LIDAR and on-site instruments provided relevant information on the evolution and properties of the plume over the central part of the Iberian Peninsula. Aerosol extinction coefficient profiles provided by the LIDAR station show the presence of remarkable aerosol layers between 6 May and 15 May. Provenance studies using Hysplit backtrajectories and EURAD model forecasts confirmed that most of the aerosol layers originated in the Eyjafjallajökull eruption. The large suite of semi-continuous instruments present in the latter site allowed a better characterization of the aerosol properties. Size distribution and chemical composition were continuously monitored during the event, revealing a large increase in the aerosol fine mode, in coincidence with increases in ambient sulfate concentration, while the coarse mode remained almost unaltered. These results show that the plume carried mainly fine particles, with sizes between 0.1 and 0.7 μm in diameter, in contrast with the usual assumption that volcanic aerosol is mainly in the range of several μm up to mm. A possible

explanation for this can be related to the long distance transport suffered by the plume and by the secondary formation of particulate sulfate from the gaseous sulfur dioxide. The information on volcanic aerosol characteristics after long-range transport, provided by this study, might be relevant for establishing a threshold for safe aircraft operation in volcanic ash.

Keywords: Eyjafjallajökull, volcanic ash, particulate sulfate, atmospheric aerosols

1. Introduction

European airspace was closed from 15 to 20 April 2010 due to the volcanic eruption at Iceland. The Eyjafjallajökull volcano (63.63ºN, 19.62ºW, 1660 m asl) had remained dormant for several decades; however, in the 1990s high seismic activity was registered (Sturkell et al, 2010; Hjaltadóttir et al, 2009). Volcanic eruptions are not uncommon in Iceland, but this one has shown characteristics different from those usually expected. Instead of peaking during the first few days and then gradually decreasing, the eruption had an explosive phase with mainly tephra and ash production, and a phase of mainly lava production before becoming explosive again (Petersen, 2010). As glaciers cover the volcano, eruptions are phreato-magmatic by nature (Sturkell et al, 2010). Phreato-magmatic eruptions arise from interactions between water and magma. Unlike magmatic eruptions, which are driven by the thermal expansion of magma, phreato-magmatic eruptions are driven by the thermal contraction of magma when it comes in contact with cold water. The temperature difference between the two causes the violent water-lava interactions that make up the eruption. On 20 March 2010 a violent eruption started, forcing the evacuation of the local population and interfering with air traffic in the region. The eruption entered a strong phase of ejection of ash to the atmosphere on 14 April 2010, with large aerosol plumes rising up to the high troposphere during the following days (14–17 April). These were rapidly advected down the North Sea and then dispersed over a very large area of central and northern Europe (Colette et al, 2010; Flentje et al, 2010), disrupting air traffic for several weeks. The eruption shifted to a lava producing phase throughout late April (18–30 April), but after more than a week of relatively subdued activity, the volcano began a new round of explosive ash eruptions in the first week of May. The meteorological conditions favored the arrival of the volcanic ash cloud at Spain. The plume crossed over the Iberian

Peninsula from West to East between 7 and 9 May, and then over the Mediterranean and the Balkans, according to model simulations.

The evolution in space and time of the volcanic plume was forecasted by several models, such as NAME (Numerical Atmospheric-dispersion Modelling Environment, Jones et al 2007), MOCAGE (Modélisaton de la Chimie Atmosphérique Grande Echelle, Josse et al. 2004), EURAD (EURopean Air Pollution Dispersion, Hass et al, 1995) or FLEXPART (Stohl et al, 2005), driven by meteorological fields along with data on concentration, composition and size of the ash particles. The ash plume was observed by a variety of ground-level and satellite sensors (SEVIRI, GOME, IASI, GOES, TOVS, AVHRR, AIRS, MODIS, SCHIAMACHY, OMI, SBUV/2, CALIOP…). The most effective ground-level measurement system for detecting the presence of volcanic plumes is LIDAR (**Li**ght **D**etection **A**nd **R**anging), which is an optical remote sensing technology that measures properties of scattered light to find range and/or other information on a distant target based on emitting laser pulses to the atmosphere and detecting the backscattered signal. However, LIDAR signals cannot penetrate thick clouds, so that low-level clouds obscure the detection of aerosol plumes higher up in the atmosphere. During the days of the event, LIDAR systems were the only remote sensing measurements from which vertically resolved mass concentrations could be estimated. The impact on air traffic, with thousand of flights cancelled, generated a demand for timely mass loading estimates in order to determine the damaging potential of the plume. A special effort was made by EARLINET (European Aerosol Research LIDAR NETwork) (Bösenberg et al, 2001) to monitor the ash plume dispersion in order to provide vertically resolved loading estimates.

The effects of volcanic ash clouds on civil aircraft are related to the dangers of jet engines ingesting material, leading to immediate loss of power. In at least one well-known incident, a British Airways Boeing 747 lost power from all four engines over Indonesia, but recovered after an emergency restart to make an emergency landing (Przedpelski and Casadevall 1994). Since then, guidelines for safe flight call for the avoidance of all encounters with ash. The “zero tolerance” of ash led directly to a sequence of decisions that reduced air traffic in European airspace to a “zero rate” in those sectors identified as contaminated. Due to the considerable disruption and economic cost of the decisions made, there was an urgent need to identify the density of ash that could be tolerated by jet engines.

On 20 April 2010, aircraft and engine manufacturers determined that engines would tolerate operations in an ash density of 2 mg m^{-3} (ICAO, 2010). In order to develop safety policies for air operation in presence of volcanogenic aerosol, a complete physico-chemical and morphological characterization of this aerosol is needed, as well as studies on its impact on airplane engines. The characteristics of the aerosol generated depend on the type of volcanic system and the eruption conditions, as well as on the transformation processes that occur later in the atmosphere. Further experimental data are required to properly address this issue.

Volcanoes are very strong sources of sulfur, acids and other gases, as well as particles. Both sulfur dioxide (SO_2) and sulfate (SO_4^{2-}) have been found in volcanic plumes. Sulfate can be either primarily emitted or result from the oxidation of gaseous SO_2 (Allen et al, 2002). A recent study has shown increasing SO_2 depletion and gas phase sulfuric acid (H_2SO_4) enrichment in the volcanic plume of an Antarctic volcano with the distance to the emission source, suggesting a fast SO_2 to SO_4^{2-} oxidation (Oppenheimer et al, 2010). It is known that sulfuric acid and sulfate aerosols are essential precursors for cloud formation over oceans (Charlson et al, 1987). This means that the sulfate aerosol generated near the source is expected to suffer subsequent processing on long-range atmospheric transport. However, the chemical stability of sulfate makes it a feasible candidate for detecting long-range transported volcanogenic aerosols. Ground-based measurements of volcanic emissions have traditionally focused on sulfur dioxide concentrations, but a few studies have also reported continuous measurements of aerosol chemical compounds of volcanogenic origin such as sulfate. In one recent work of this type (Ovadnevaite et al, 2009) the authors also demonstrated that a large amount of sulfur released from Icelandic volcanoes could travel over distances greater than 1,000 Km.

Here we report measurements of volcanogenic aerosols at ground level, identified by an increase in gaseous SO_2 and particulate sulfate concentrations in several background air pollution Spanish monitoring stations of the Iberian Peninsula, and detailed observations of the ash layer over Madrid provided by a ground-based Raman LIDAR during the aforementioned event in May. The CIEMAT-Madrid LIDAR station forms part of EARLINET and provided timely measurements from the beginning of the event. This station also has a suite of semi-continuous instrumentation for measuring surface aerosol

properties and meteorological parameters. The PM_{10}, $PM_{2.5}$ and PM_1 temporal evolution and mass distributions, along with particulate sulfate temporal evolution, have been obtained.

2. Experimental Setup

2.1. Measurement sites

2.1.1. EMEP/GAW/CAMP network

The Iberian Peninsula is located in the southwestern part of Europe, about 2800 Km south-southeast of the Eyjafjallajökull volcano. EMEP/GAW/CAMP is the Spanish network for monitoring reactive gases, particulate matter and chemical precipitation under the EMEP (**E**uropean **M**onitoring and **E**valuation **P**rogramme), CAMP (**C**omprehensive **A**tmospheric **M**onitoring **P**rogramme) and GAW (**G**lobal **A**tmospheric **W**atch of the World Meteorological Organization) Programmes, and is managed by the Spanish Meteorological Agency (AEMET). It is formed by 13 stations located throughout the Iberian Peninsula and the Balearic Islands. The names and locations of the operative Spanish network stations are presented in Figure 1.

(Approximate location of Figure 1)

(Approximate location of Table I)

2.1.2. CIEMAT site (Madrid)

The Madrid Metropolitan Area is located in the center of the Iberian Peninsula, bordered to the north–northwest by a high mountain range (Sierra de Guadarrama) 40 km from the city, and to the northeast and east by lower mountainous terrain. The population of the metropolitan area of Madrid is nearly 6 million inhabitants, with a car fleet of almost 3 million vehicles. Since its industrial activity consists essentially of light factories, the Madrid plume is typically urban, fed by traffic emission and also by domestic heating in winter. Previous studies of air pollution episodes in the Madrid air basin have characterized their driving meteorological conditions and their typical transport patterns (Plaza et al., 1997; Pujadas et al., 2000; Artíñano et al., 2003). The general synoptic situation leading to the occurrence of episodic events corresponds in winter to stagnant anticyclone conditions, light winds and clear-sky conditions, with the usual formation of radiative nocturnal surface inversions. In spite of the local-regional transport pattern, the great distance between the Madrid metropolitan area and other significant urban or industrial areas in Spain (around

1200 km) allows the study of its plume as a typical urban plume. Long-range transport
2episodes significantly affecting aerosol concentrations in the Madrid region are usually
3limited to Saharan mineral dust intrusions (Salvador et al., 2004). The arrival of Atlantic or
4polar air masses generally has a cleansing effect on the atmosphere, significantly reducing
5particulate matter levels.
6Located in the Madrid NW city outskirts, the CIEMAT area can be considered as an urban
7background or suburban site. It is situated downwind of the city for N to SW wind
8directions and downwind of a great forested area for W to NW wind directions.
9Simultaneous vertical profiles and surface aerosol concentration measurements were
10carried out within this site.

11**2.2 Instrumentation**

12The EMEP/GAW/CAMP network takes samples of particulate matter filters in 24-h
13periods, from 07:00 to 07:00 UTC, using the techniques detailed in Table I. The samples
14are subject to chemical analyses in the laboratory of the Carlos III Health Institute.
15Particulate sulfate and nitrate concentrations are determined by Ion Chromatography.
16Sulfur dioxide is continuously monitored at each of the EMEP/GAW/CAMP sites with UV
17pulsed fluorescence analyzers. Due to technical problems some data are missed along these
18days, in a few stations.
19At the CIEMAT site (Madrid), a ground-based Raman LIDAR station belonging to
20EARLINET is in regular operation. During the days of the event a special effort was made
21by EARLINET (European Aerosol Research LIDAR NETwork) to monitor the ash plume
22dispersion in order to provide vertically-resolved measurements that decision-makers
23required as soon as possible. The LIDAR system is a laboratory equipment based on a
24Nd:YAG laser source (Spectra Physics LAB170-30) operating at the 2nd harmonic (532
25nm), a 30 cm diameter Newtonian telescope and photon-counting acquisition system. The
26laser energy was 115 mJ/pulse, operated vertically due to safety reasons. Other instrument
27characteristics have been described elsewhere (Molero and Jaque, 1999). LIDAR signals
28are recorded with 1-minute resolution (1800 laser pulses), but later 30- to 60-minute files
29are averaged in order to derive vertically a resolved aerosol extinction coefficient profile
30with adequate SNR values. The Klett-Fernald algorithm (Klett, 1981) is used in the
31inversion, with an aerosol extinction-to-backscatter ratio of 50 sr (continental aerosols).

The Rayleigh extinction coefficient was calculated based on the revision of the theory (Bodhaine et al., 1999) using vertical profiles of meteorological data from the nearby AEMET radiosonde station at the Barajas airport.

The LIDAR was co-located with a suite of semi-continuous instrumentation for measuring surface aerosol properties and meteorological parameters. The temporal evolution of particle number, sulfate and mass concentration for particles smaller than 10, 2.5 and 1 μm diameter (PM_{10}, $PM_{2.5}$, PM_1) were also obtained at surface level in the CIEMAT site. Time series of particulate sulfate on PM_1 were obtained by means of a Thermo 5020 sulfate particulate analyzer (SPA) (Schwab et al, 2006) on a time basis of 20 minutes. The instrument reduces sulfate aerosol by thermal catalysis and analyzes the resulting sulfur dioxide gas by pulsed fluorescence. Laboratory conversion efficiencies have been proved to be higher for ammonium sulfate than for mineral-type sulfates. The measurements were corrected by comparison against daily filter-based measurements.

Particulate nitrate concentrations on $PM_{2.5}$ were semi-continuously measured by the Rupprecht and Patashnick Series 8400N Ambient Particulate Nitrate Monitor every 10 min. (Long and McClenny, 2006). This instrument comprises a pulse generator for the collection and vaporization of the particulate matter and a NOx pulse analyzer. It mainly measures the nitrate associated with the ammonium, mineral-type nitrates being refractory to this technique. These measurements were also corrected by comparison with daily filter-based measurements.

Two optical particle counters (OPC), models GRIMM1108 and GRIMM1107, characterized the aerosol properties at ground level. GRIMM1108 OPC provides size distribution in the range from 0.3 to 20 μm. Each particle is sized by the amount of incident laser light scattered at an angle of 90º, obtaining a 15-channel particle number concentration by optical size. (Peters et al, 2006). These data, in the form of particle counts, may be converted to a volume distribution (based on the particulate matter diameter) or a mass distribution. In calculating the latter, particulate density information is required. Generally, this information is not available, so that a uniform density is assumed. According to the manufacturer, the reproducibility of the GRIMM1108 in particle counting is +/- 2%. GRIMM1107 OPC employs 31 channels to obtain a similar distribution, which is converted into a mass distribution by the internal software. The particle diameter data are

first converted to particle volume assuming spherical particles, and then these volume data are converted to mass distribution using a constant density factor, resulting in a PM_{10}-$PM_{2.5}$-PM_1 mass distribution. (Grimm and Eatough, 2009). Both instruments incorporate a heater at the sample inlet with the purpose of drying the aerosol. GRIMM1107 also incorporates a silica gel dryer. Data were recorded every 10 min by both instruments.

The particle size distribution in the particle size range 0.015-0.60 μm was measured using a Scanning Mobility Particle Sizer (TSI SMPS 3936 instrument), combining a long Differential Mobility Analyzer (DMA) and a Condensation Particle Counter (CPC model 93775), and working in the scanning mode (Wang and Flagan, 1990). Before entering the DMA the sample was dried by a nafion drier, and particles were neutralized by a Kr-85 radioactive source. Once in the DMA, particles were classified according to their electrical mobility and then counted by the CPC.

The GRIMM1108 and the SMPS overlap in the size range from 0.3 μm (lower size end of the GRIMM1108) to 0.661 μm (upper size end of the DMA) resulting in a 22 bin overlap region spanning $0.311 < D_p < 0.661$ μm for DMA and a 3 bin overlap region spanning $0.3 < D_p < 0.6$ μm for the GRIMM1108. Therefore, it is possible to obtain a single plot for number distributions from 0.015 to 20 μm by joining the data of both instruments under some assumptions. The diameter of a particle can be determined by measuring different physical properties such as light scattering or electrical mobility. SMPS classifies particles according to their electrical mobility. Particles of equal Stokes diameter D_p that carry the same electrical charge will have the same electrical mobility. Hence, for spherical particles, the electrical mobility diameter would equal D_p. D_p, which is independent of density, is also used in size distributions based on light scattering. For spherical particles, the diameter given by optical particle counters will equal D_p if light absorption is negligible and the refractive index is constant for the GRIMM1108 distribution. Mass concentrations ($dM/d\log(D_p)$) were calculated assuming that aerosol particles were spheres with a diameter equal to the center diameter of each bin measured by the instruments.

Meteorological information in Madrid was obtained from a permanent tower installed at CIEMAT with the following parameters and heights: wind direction and speed at 52 m agl, precipitation and solar radiation at 31 m agl, temperature and humidity at 4m agl and pressure at ground level. Data were recorded every 10 min.

Air mass back trajectories were calculated using two models: the Hybrid Single-Particle Lagrangian Integrated Trajectory (HYSPLIT) dispersion model (Draxler and Rolph, 2010), and the FLEXTRA model (Stohl et al, 1995) installed in AEMET driven by the meteorological analyzed fields from the HIRLAM/AEMET NWP operational suite.

3. Results and discussion

3.1. Remote sensing and model results

The eruption of the Eyjafjallajökull volcano, which started on March 20, went through several explosive phases followed by lava production before the final degassing phase, about two months later. In these explosive phases aerosol release to the atmosphere was highly enhanced, representing the greatest risk to air traffic. The volcanic event that started on 14 April affected mainly the British Isles and Central Europe. A new round of explosive ash eruptions occurred in the first week of May. The HIRLAM/AEMET meteorological fields analysis at 500 hPa depicts a strong ridge over the West of Iceland located between two depressions, one of them over Newfoundland whereas the other one over the Balearic Islands. This situation favored the arrival the volcanic plume at the Iberian Peninsula. The plume crossed over the Iberian Peninsula from West to East between 7 and 9 May, and several ash layers could be detected over Madrid by LIDAR. Measurements in the time period from 4 to 14 May were analyzed.

(Approximate location of Figure 2)

Figure 2 shows the first signs of arrival of the volcanic ashes over Madrid, observed on 6 May at 00:00 UTC by means of the LIDAR system in a double layer located between 4.5 and 5.4 Km asl (bottom left panel) The bottom right panel shows color-coded plots of the range-corrected LIDAR signals averaged to obtain the extinction coefficient profile, where the vertical axis is the same as in the previous panel and the horizontal axis represents time (bottom left panel). The provenance of these layers is confirmed by the backtrajectories provided by Hysplit model ending over Madrid at 2500 m (red), 5000 m (blue) and 7500 m (green) on 6 May 00:00 UTC plotted on Google Earth (top left panel). On this panel, the MODIS image from the near real-time “rapidfire” website service obtained on 2 May, 12:20 UTC is also plotted on Google Earth. This image was selected as the one out of the images available closest in time to the situation of the volcano when the ashes that reached

Madrid on the 6 May at 00:00 UTC were emitted, which is roughly on 3 May at 00:00 UTC according to the backtrajectories analysis. The image shows the ash from the plume blowing toward the east-southeast, passing over a charcoal-colored ash field on the land surface. Figure 2 also shows the 3-km height plume dispersion provided by the EURAD model (top middle panel), which indicates that the ash plume reached only the north-west of the Iberian Peninsula, while faint traces of it were being detected over Madrid.

As mentioned in the introduction, one of the most critical parameters for aviation is aerosol mass concentration, so that there was a demand for timely mass loading estimates during the volcanic event in order to determine the damaging potential of the ash plume on jet engines. LIDAR systems were the only remote sensing measurements from which vertically resolved mass concentration could be estimated, although large uncertainties remain in the conversion from extinction coefficient to mass concentration profiles. In this work the extinction coefficient profiles were converted into mass concentration profiles using a so-called specific extinction coefficient or cross section value of 0.64 $m^2 g^{-1}$ at 550 nm, provided by the OPAC (Optical Properties of Aerosol and Clouds) software (Hess et al., 1998), assuming that the refractive index of volcanic ash is close to that of mineral dust and that the refractive index of sulfate droplets is close to that of water soluble aerosols. The bottom left panel of figure 2 shows the extinction coefficient profile provided by the LIDAR system, with a mixing layer up to 2.5 Km, and a double-sided ash layer between 4.5 and 5.4 Km, with a maximum value of 1.83 x 10^{-5} (±0.32) m^{-1} (bottom x-axes). This value converts into a mass concentration value of 28.6 (±5) $\mu g\ m^{-3}$ (top x-axes), well below the potential hazardous values of 2 mg m^{-3} considered by aircraft and engine manufacturers. The error assigned to the mass concentration value corresponds to the experimental error estimated for the extinction coefficient, but due to the aforementioned uncertainties regarding the specific extinction coefficient, this error can be significantly larger. However, no further estimates can be made for it with the data available.

(Approximate location of Figure 3)

Figure 3 shows the moment at which the volcanic ash layers reached the highest optical depth observed during the whole event. This occurred on 7 May, at 01:00 UTC in several layers located between 4 and 6.5 Km asl. The extinction coefficient peak reached 4.93 x 10^{-5} (±0.63) m^{-1}, corresponding to a maximum detected value for volcanic layers of 77 (±9.6)

1µg m^{-3}. Therefore, the maximum mass concentration detected is well below the critical
2limits considered by the U.S. military (50 mg m^{-3}), and even below the reduced values
3suggested by aircraft and engine manufacturers during the event (2 mg m^{-3}). The
4provenance of those layers is again confirmed by the backtrajectories provided by the
5Hysplit model ending over Madrid at 2500 m (red), 5000 m (blue) and 7500 m (green) on 7
6May 01:00 UTC plotted on Google Earth (top left panel). The MODIS image, obtained on 4
7May, 14:00 UTC, shows the ash from the volcano extending 300 to 400 km southeast. The
8ash plume on 4 May reached a height of 5.8 to 6.0 km above sea level, estimated from the
9Icelandic Coast Guard flight at 10:40 and 15:30 GMT and had spread 65 to 80 km east-
10southeast of the volcano. The south-blowing ash resulted in flights being cancelled in
11Ireland and Scotland on 5 May. It reached Madrid two days later. The 3-km height plume
12dispersion provided by EURAD model (top middle panel) correctly predicts ash layers over
13Madrid. Several layers were detected during the day, slowly subsiding towards the mixing
14layer, but low clouds interfered the measurements at some times. During 7 and 8 May,
15volcanogenic particles were detected at ground level in Madrid and at several
16EMEP/GAW/CAMP stations, as will be explained further below.
17 (Approximate location of Figure 4)
18Figure 4 depicts the situation 26 hours after the maximum ash layers were detected. In this
19case, a mixing layer is observed up to 2.8 km and residual ash layers are detected between 4
20and 6.9 km, with extinction coefficient values below 0.4 x 10^{-5} m^{-1}. The air masses seem to
21come from North of the British Isles but not directly from Iceland, according to the
22backtrajectories provided by Hysplit model ending over Madrid on 8 May 03:00 UTC (Top
23left panel). The MODIS image, obtained on 6 May, 11:55 UTC, shows a thick plume of ash
24blowing east and then south from the volcano. Clouds bracket the edges of the scene, but
25the dark blue waters of the Atlantic Ocean show in the middle, and above them, a rippling,
26brownish-yellow river of ash. The 3-km height plume dispersion provided by EURAD
27model (Top middle panel) shows how the plume was moving east after passing over
28Madrid. No further measurements were possible after this, due to low clouds and rain
29caused by a clean air mass from the Atlantic Ocean that washed the atmosphere from the
30West. The clean atmosphere observed over Madrid 7 hours before volcanogenic aerosols

were detected at the CIEMAT site, highlights the inherent difficulty of characterizing the plume from a single LIDAR station.

(Approximate location of Figure 5)

Figure 5 shows another event detected five days later. In this case, a mixing layer with clouds on top is observed up to 3 km and a double-sided ash layer is detected between 4.5 and 5.5 km, with extinction coefficient values around 1.25 x 10^{-5} (±0.53) m^{-1}, corresponding to a mass concentration value of 19.5 (±8.3) μg m^{-3}. Although in this case backtrajectories indicate Icelandic provenance, the 3-km height plume dispersion provided by EURAD model (Top middle panel) and the MODIS image, obtained on 12 May, 14:45 UTC over the Atlantic, suggest contribution from an Atlantic airmass polluted with volcanic aerosols from previous days. A minor event was detected at ground-level on the evening of 13 May, as it will be explained below.

3.2. Ground based measurements

Sulfur dioxide is a major component of volcanic clouds and subsequently sulfuric acid may be formed by photochemical conversion, thus giving rise to secondary sulfate formation. Accordingly, volcanic ash plumes are generally formed by gaseous pollutants, mainly SO_2, primary ash particles (micrometer size range) and also secondary smaller particles (nanometer size range). Thus, it is interesting to jointly investigate gases, fine and coarse aerosols to know the spatial distribution of the different kind of pollutants produced at the eruption.

The passage of the volcanic ash plume over the Iberian Peninsula was detected at ground level in most EMEP/GAW/CAMP stations, mainly during three days, from 7 to 9 May 2010, although the first effects were recorded on 2 May at O Saviñao and 4 May on several stations. In this period, high pressure atmospheric circulation over the Atlantic favored subsidence. There was rainfall irregularly distributed through Spain, which in some cases could contribute to wet deposition of pollutants by precipitation scavenging and then reduce observed gaseous pollutants and particulate matter in ambient air. There was no rain at Doñana and Els Torms, whereas it rained heavily at Noia. The rainfall was accompanied by storms that persisted in the following days with variable intensity. The analysis of precipitation samples of these days, collected in 24-hours periods, shows enhanced values

of sulfate. In Noia and O Saviñao, the highest concentration of sulfates in precipitation samples occurred on 6 May 2010.

The first sign of volcanic impact is a rise in SO_2 concentrations, which is not correlated with a similar pattern of other anthropogenic pollutants such as nitrogen oxides and ozone. A sulfur dioxide peak appeared at O Saviñao on 2 May and other noteworthy peaks were detected on 4 May at this site, 13:30 UTC, Peñausende at 15:00 UTC, San Pablo at 15:30 UTC and Víznar, on 5 May at 00:00 UTC. Figure 6 shows the temporal evolution of SO_2 at San Pablo de los Montes (ES01), Víznar (ES07), Zarra (ES12) and Els Torms (ES14), between 4 and 14 May 2010. These are the stations where SO_2 maxima not connected with high values of the other pollutant gases (not shown on the figure for clarity), can bee seen more clearly during this period. Ash plume effects appeared from West to East of Spain so that the main values were recorded as follows: San Pablo on 7 May, at 17:00 UTC; Víznar on 8 May at 11:00 UTC; Zarra, on 8 May at 16:00 UTC; and Els Torms on 9 May at 8:00 UTC. At other stations the origin of SO_2 peaks is disguised by the presence of high values of NOx; no influence is observed at the Cabo de Creus and Mahón stations. FLEXTRA air mass backtrajectories calculated in AEMET show that the Cabo de Creus and Mahón stations were out of the influence of the air mass coming from South Iceland. In addition, the model proves that this air mass reached Els Torms later than the rest of the sites.

(Approximate location of Figure 6)

Figure 7 shows the PM_{10} and $PM_{2.5}$ mass concentrations in the top panel, PM_{10}-sulphate, PM_{10}-nitrate (24-h averages) concentrations (middle panel) and the S/N ratio (bottom panel) from 4 to 14 May at the Zarra station. Another consequence of a volcanic eruption is the increased mass concentration of particles in coincidence with high levels of sulfate ion concentration in them. Although the PM_{10} and $PM_{2.5}$ mass concentrations recorded by the EMEP/GAW/CAMP Network during this period were not at unusually high values, at most of the sites relative maxima are observed and sulfate content in PM_{10} presents very high values together with very low values of nitrates. Therefore, the S/N ratio (where S is sulfur as sulfate and N is nitrogen as nitrate) obtained in daily PM_{10} filters is high at almost all of the stations of the network. This ratio allows identifying these peaks as volcanogenic aerosols. Filter probes were not taken on 7 May at O Saviñao and on 8 May at Noia. At O Saviñao the S/N ratio stands out on 6 May, the same date of the maximum sulfate in

precipitation. The situation was clearer at Barcarrota, Peñausende, San Pablo, Víznar, Zarra, and Els Torms. At the first sites, maxima concentrations were recorded on 8 May, while at Els Torms station the maximum happened on 9 May. The behavior is the same as that previously described for sulfur dioxide, and agrees with FLEXTRA backtrajectories model results. The Campisábalos station is the only one in which chemical composition of 24-hours $PM_{2.5}$ filters was obtained, on a weekly basis. The sulfate level on 8 May is an annual maximum and coincides with a minimum in nitrates. This ratio is similar for PM_{10} filters since high levels of sulfates coincide with very low values of nitrates in this period.
(Approximate location of Figure 7)

In figure 8, the temporal evolution of the particle mass concentration and particulate sulfate and nitrate concentration at the CIEMAT site between 4 and 14 May is depicted together with relative humidity (RH) and rain, meteorological parameters with a clear influence on particle concentration.

(Approximate location of figure 8)

The first remarkable sulfate peak appears on 4 May at 13:00 UTC, in coincidence with the sulfur dioxide peaks observed at the O Saviñao, Peñausende and San Pablo EMEP/GAW/CAMP stations. PM_1 sulfate concentration increases sharply during 4 hours, while RH remains at low values. On the evening of 4 May the concentration descends. Nevertheless, the previous level is not recovered until 5 May in the afternoon. The percentage of sulfate in PM_1 increases by 20% during this event.

During the morning of 7 May a significant PM_{10} peak simultaneously with an increase in particulate nitrate levels and no remarkable fine sulfate increases were observed. This pollution event, not related with the arrival of volcanic ash, can be compared with the sharp increase in PM_1 sulfate levels that took place on 8 May at 11:00 UTC, and five hours later sulfate reached a maximum of 3 $\mu g\ m^{-3}$. This value is more than three times higher than the average level of 2010 (0.72 $\mu g\ m^{-3}$) and 3 times higher than the 80th percentile. The sulfate concentration in PM_1 increased 20% during the rise of the peak. RH at this time remained below 65% at all times, so this increase cannot be attributed to hygroscopic sulfate formation. As mentioned previously, sulfate peaks were observed at the San Pablo, Víznar and Zarra stations on this day. At the CIEMAT site, particulate sulfate concentrations remained steady until the early hours of 9 May, when the aerosol was removed by rain

scavenging. This increase is also seen in PM_1 concentration, reflecting both the sulfate event and also the later increase in nitrate levels. Results suggest that the hygroscopic nitrate formation was due to the high RH levels starting after the sulfate concentration reached its maximum. Hygroscopic nitrate formation has already been detected at this site in previous studies (Gomez-Moreno et al, 2007). The aerosol coarse fraction was not affected during this event.

From 7 to 14 May, PM_1 contribution remained a major fraction of PM_{10}. During this period model results show prevailing wind flows from northern Europe. On the evening of 13 May a second noticeable sulfate event took place. Shortly after a rain event the concentration tripled its value in less than three hours, falling again at midnight. The increase in the percentage of sulfate in PM_1 was similar to the events of 4-5 and 7-9 May, but in this case RH values remained over 70%. No nitrate production was detected and coarse particulate matter did not suffer any significant change. The shorter time period and smaller values attained by this event might explain why it was not detected at the EMEP/GAW/CAMP network, where samples are averaged in 24-h periods.

Figures 9 and 10 depict mass distributions, obtained from both SMPS and OPC instruments, exhibiting a bimodal size distribution in the range 0.1 – 20 μm. SMPS gives number distribution from 0.015 to 0.661 μm, while OPC gives number distribution from 0.3 to 20 μm. Mass concentrations ($dM/d\log(D_p)$) were calculated under the assumptions mentioned in the instrumentation section. A constant aerosol density of 1.5 g m^{-3} was considered for all size fractions. This is an average value for urban aerosols found in different works (Pitz et al, 2003; Geller et al, 2006). The overlap region shows some discrepancies due to the different techniques employed. However, the results are consistent. Lognormal distributions were fitted to the fine mode and coarse mode separately. Values for geometric diameter (d_g) and geometric standard deviation (σ_g) of the distributions, given by the fitting algorithm, are shown in Table II. The mode (D_p) was obtained from these parameters using the Hatch-Choate equations (Hinds, 1982), and is also shown in Table II.

(Approximate location of Table II)

(Approximate location of Figure 9)

Figure 9 shows the distributions measured on 7 May at 12:00 (squares), on 8 May at 0:00 (circles) and on 8 May at 18:00 (triangles). The first situation occurred during the local pollution event mentioned before, with a large increase in PM_{10} and nitrate concentration values but not affecting PM_1 levels. The nitrate concentration increase reveals the anthropogenic origin of pollutants. The second case reflects a clean atmosphere, with low values of all parameters measured. In both cases the fine mode was located at 0.25 μm, as can be seen in table II. However, when the volcanic event was detected at ground level the mode is displaced to 0.39 μm. The coarse distribution was similar under the clean and volcanic cases, being significantly higher in magnitude and size mode for the local event. Between 7 and 9 May an increase in the fine mode caused by the arrival of the volcanogenic aerosol can be clearly seen. Nevertheless, aerosol size at 18:00 might already reflect some secondary production due to hygroscopicity since rising RH values reached 75% around that time. Previous works have stated hygroscopic secondary aerosol production at RH levels over 70% (Chen et al, 2003).

Figure 10 shows the distributions calculated for the second sulfate event. On 13 May at 6:00 (black squares) a local PM_1 event takes place. Again, the increase in nitrate indicates an anthropogenic event. On 13 May at 18:00, another volcanogenic event was identified by the sulfate peak without nitrate concentration increased. Finally, on 14 May at 0:00, the event has nearly ceased and values reflect a clean atmosphere. In the first and last cases the fine mode of the distribution is under 0.25 μm, while during the sulfate event it grows to over 0.30 μm. The coarse fraction presents a small contribution to the aerosol in all three cases. On 13 and 14 May, an increase in the fine mode is seen again during the sulfate event. RH is over 80% in the three moments studied, before, during and after the event, so that by itself it cannot explain the increase in aerosol size.

(Approximate location of Figure 10)

Size distributions of ions present in aerosols sampled at ground level near volcanoes have been obtained by other researchers, finding a major sulfate mode of 0.5 μm (Mather et al, 2003) and 0.1-0.25 μm (Ilyinskaya et al, 2010). In both cases the importance of background meteorological conditions for particle evolution was stated, observing an increase in sulfate

aerosol size in high humidity conditions for the former. Our results are consistent with these, showing a mode D_p of 0.39 μm when volcanogenic sulfate aerosol impacts on the ground. This value is distinguishable from the local accumulation mode, typically with a D_p on the order of 0.25 μm. No impact is seen on the coarse aerosol mode, thus suggesting the removal of the larger ash particles before the arrival of the plume at the sampling point.

4. Conclusions

We present results on the aerosol characteristics of the volcanic ash emitted by the Icelandic volcano Eyjafjallajökull during May 2010 and detected at several sites of the Iberian Peninsula. Ground-based on-site observations from the Spanish EMEP/GAW/CAMP network were affected by the volcanic ash plume from the eruption of the Eyjafjallajökull volcano. The concentrations of sulfur dioxide and sulfate in PM_{10}, $PM_{2.5}$ and precipitation reached relative maxima independently of high values of other pollutants such as nitrogen oxides and ozone. The first effects appeared on 4 and 5 May from the northwest to the southeast of Spain, but they intensified between 7 and 9 May at the sites in the center and south of the Iberian Peninsula. In this period no influence was detected in the Eastern Spain stations, Cabo de Creus and Mahón. In the northwestern stations of Noia and O Saviñao the relative maximum of sulfate in precipitation occurred on 6 May, as did PM_{10} at O Saviñao, where there was no PM_{10} filter on 7 May. In the rest of the period, sulfate values in PM_{10} are not remarkable, either because of the removal of pollutants by wet deposition or because of a lower influence of the plume in this zone. At the CIEMAT site (Madrid), an estimation of the vertical profiles of mass concentration was calculated from the extinction coefficient profiles, obtaining maximum values (77 (±9.6) μg m^{-3}) well below the threshold established for safe aircraft operation. In this site the size distribution and chemical composition were continuously monitored during the event, detecting a large increase in the aerosol fine mode in coincidence with an increase in sulfate concentration, while the coarse mode remained almost unaltered. Mass distributions at ground level indicate particles mainly in the 0.1-0.7 μm size range. These results contrast with the usual assumption of volcanic aerosol mainly in the range of several μm up to mm. A possible explanation for this can be related to the long distance transport suffered by the plume and the secondary formation of particulate sulfate from gaseous sulfur dioxide. The information

on volcanic aerosol characteristics after long-range transport provided by this study might be relevant for establishing a threshold for safe aircraft operation when volcanic ash is present.

Acknowledgments

This work is supported by Spanish Ministry MICINN through the project PROFASE (CGL2007-64117-CLI), the complementary action CGL2010-09225-E/CLI and by the European Union under the project EARLINET-ASOS (EU Coordination Action, contract nº 9025991 (RICA)). The authors gratefully acknowledge the NOAA Air Resources Laboratory (ARL) for the provision of the HYSPLIT transport and dispersion model and/or READY website (http://www.arl.noaa.gov/ready.php) used in this work. Also, The Rhenish Institute for Environmental Research of the University of Cologne is acknowledged for providing the EURAD model results used in this study. The original FLEXTRA air mass trajectories model software installed and running on the AEMET computing facilities has been kindly provided by Stohl and others and downloaded from their webpage: http://zardoz.nilu.no/~andreas/flextra+flexpart.html. The Carlos III Health Institute, under agreement with AEMET, is the responsible for the chemical analysis of the PM and precipitation samples taken daily at the EMEP Spanish stations. M.A. Revuelta acknowledges the Ministry of Science and Innovation for their economical support through the FPI predoctoral grant BES-2008-007079.

References

Allen, A. G., Oppenheimer, C., Ferm, M., Baxter, P. J., Horrocks, L. A., Galle, B., McGonigle, A. J. S., Duffell, H. J. (2002). Primary sulfate aerosol and associated emissions from Masaya Volcano, Nicaragua. Journal of Geophysical Research-Atmospheres 107(D23).

Artinano, B., Salvador, P., Alonso, D. G., Querol, X., Alastuey, A. (2003). Anthropogenic and natural influence on the PM10 and PM2.5 aerosol in Madrid (Spain). Analysis of high concentration episodes. Environmental Pollution 125(3): 453-465.

Bodhaine, B. A., Wood, N. B., Dutton, E. G., Slusser, J. R. (1999). On Rayleigh optical depth calculations. Journal of Atmospheric and Oceanic Technology 16(11): 1854-1861.

Bösenberg, J., A. Ansmann, J.M. Baldasano, D. Balis, Ch. Böckmann, B. Calpini, A. Chaikovsky, P. Flamant, A. Hagard, V. Mitev, A. Papayannis, J. Pelon, D. Resendes, J. Schneider, N. Spinelli, Th. Trickl, G. Vaughan, G. Visconti, M. Wiegner (2001). EARLINET: A European Aerosol Research Lidar Network, in A. Dabas, C. Loth, and J. Pelon (eds.), Advances in Laser Remote Sensing, pp. 155–158. ISBN 2-7302-0798-8

Charlson, R. J., Lovelock, J. E., Andreae, M. O., Warren, S. G. (1987). Oceanic Phytoplankton, Atmospheric Sulfur, Cloud Albedo And Climate. Nature 326(6114): 655-661.

Chen, Lu-Yen, Jeng, Fu-Tien, Chen, Chih-Chieh, Hsiao, Ta-Chih. (2003). Hygroscopic behavior of atmospheric aerosol in Taipei. Atmospheric Environment 37(15): 2069-2075.

Colette, A., Favez, O., Meleux, F., Chiappini, L., Haeffelin, M., Morille, Y., Malherbe, L., Papin, A., Bessagnet, B., Menut, L., Leoz, E., Rouïl, L. Assessing in near real time the impact of the April 2010 Eyjafjallajökull ash plume on air quality, Atmospheric Environment (2010), doi: 10.1016/j.atmosenv.2010.09.064

Draxler, R. R. a. R., G.D. Website. (2010). HYSPLIT (HYbrid Single-Particle Lagrangian Integrated Trajectory) Model access via NOAA ARL READY , from http://ready.arl.noaa.gov/HYSPLIT.php

Flentje, H., Claude, H., Elste, T., Gilge, S., Kohler, U., Plass-Dulmer, C., Steinbrecht, W., Thomas, W., Werner, A., Fricke, W. (2010). The Eyjafjallajokull eruption in April 2010-detection of volcanic plume using in-situ measurements, ozone sondes and lidar-ceilometer profiles. Atmospheric Chemistry and Physics 10(20): 10085-10092.

Geller, M., Biswas, S., Sioutas, C. (2006). Determination of particle effective density in urban environments with a differential mobility analyzer and aerosol particle mass analyzer. Aerosol Science and Technology 40(9): 709-723.

Gomez-Moreno, F. J., Nunez, L., Plaza, J., Alonso, D., Pujadas, M., Artinano, B. (2007). Annual evolution and generation mechanisms of particulate nitrate in Madrid. Atmospheric Environment 41(2): 394-406.

Grimm, H. and D. J. Eatough (2009). Aerosol Measurement: The Use of Optical Light Scattering for the Determination of Particulate Size Distribution, and Particulate Mass, Including the Semi-Volatile Fraction. Journal of the Air & Waste Management Association 59(1): 101-107.

Hass, H., Jakobs, H. J., Memmesheimer, M. (1995). Analysis Of A Regional Model (Eurad) Near-Surface Gas Concentration Predictions Using Observations From Networks. Meteorology and Atmospheric Physics 57(1-4): 173-200.

Hess, M., Koepke, P., Schult, I. (1998). Optical properties of aerosols and clouds: The software package OPAC. Bulletin of the American Meteorological Society 79(5): 831-844.

Hind, W. C., (1982). Aerosol Technology. Properties, Behaviour and Measurement of Airborne Particles, in: John Wiley and Sons (Eds.), Wiley Interscience, pp. 91-100.

Hjaltadóttir, S., Vogfjörð, K. S., Slunga, R. (2009). Seismic Signs of Magma Pathways through the Crust in the Eyjafjallajökull volcano, South Iceland. Icelandic Meteorological Institute. Technical report.

ICAO (International Civil Aviation Organization) (2010). Ash concentration thresholds: background and future action International Volcanic Ash Task Force Working paper IVATF/1-WP/4. www2.icao.int/en/anb/met-aim/met/ivatf (December 2010).

Ilyinskaya, E., Oppenheimer, C., Mather, T. A., Martin, R. S., Kyle, P. R. Size-resolved chemical composition of aerosol emitted by Erebus volcano, Antarctica. Geochemistry Geophysics Geosystems 11: 14.

Jones A-R-, Thompson D.J., Hort M. and Devenish B. (2007). The U.K. Met Office's next-generation atmospheric dispersion model, NAME III, in Borrego C. and Norman A.-L. (Eds.) Air Pollution Modeling and its Application XVII (Proceedings of the 27th NATO/CCMS International Technical Meeting on Air Pollution Modelling and its Application), Springer, pp. 580-589.

Josse, B., Simon, P., and Peuch, V. H. (2004). Radon global simulations with the multiscale chemistry and transport model MOCAGE, Tellus 56B, 339-356.

Kannosto, J., Virtanen, A., Lemmetty, M., Makela, J. M., Keskinen, J., Junninen, H., Hussein, T., Aalto, P., Kulmala, M. (2008). Mode resolved density of atmospheric aerosol particles. Atmospheric Chemistry and Physics 8(17): 5327-5337.

Klett, J. D. (1981). Stable Analytical Inversion Solution for Processing Lidar Returns. Applied Optics 20(2): 211-220.

Long, R. W. and W. A. McClenny (2006). Laboratory and field evaluation of instrumentation for the semicontinuous determination of particulate nitrate (and other

water-soluble particulate components). Journal of the Air & Waste Management Association 56(3): 294-305.

Mather, T. A., Allen, A. G., Oppenheimer, C., Pyle, D. M., McGonigle, A. J. S. (2003). Size-resolved characterisation of soluble ions in the particles in the tropospheric plume of Masaya volcano, Nicaragua: Origins and plume processing. Journal of Atmospheric Chemistry 46(3): 207-237.

Molero, F. and F. Jaque (1999). The laser as a tool in environmental problems. Optical Materials 13(1): 167-173.

Oppenheimer, C., Kyle, P., Eisele, F., Crawford, J., Huey, G., Tanner, D., Kim, S., Mauldin, L., Blake, D., Beyersdorf, A., Buhr, M., Davis, D. (2010). Atmospheric chemistry of an Antarctic volcanic plume. Journal of Geophysical Research-Atmospheres 115: 15.

Ovadnevaite, J., Ceburnis, D., Plauskaite-Sukiene, K., Modini, R., Dupuy, R., Rimselyte, I., Ramonet, M., Kvietkus, K., Ristovski, Z., Berresheim, H., O'Dowd, C. D. (2009). Volcanic sulfate and arctic dust plumes over the North Atlantic Ocean. Atmospheric Environment 43(32): 4968-4974.

Peters, T. M., Ott, D., O'Shaughnessy, P. T. (2006). Comparison of the Grimm 1.108 and 1.109 portable aerosol spectrometer to the TSI 3321 aerodynamic particle sizer for dry particles. Annals of Occupational Hygiene 50(8): 843-850.

Petersen, G. N. (2010). A short meteorological overview of the Eyjafjallajokull eruption 14 April-23 May 2010. Weather 65(8): 203-207.

Pitz, M., Cyrys, J., Karg, E., Wiedensohler, A., Wichmann, H. E., Heinrich, J. (2003). Variability of apparent particle density of an urban aerosol. Environmental Science & Technology 37(19): 4336-4342.

Plaza, J., Pujadas, M., Artinano, B. (1997). Formation and transport of the Madrid ozone plume. Journal of the Air & Waste Management Association 47(7): 766-774.

Przedpelski, Z. J., and Casadevall, T. J. Impact of volcanic ash from 15 December 1989 Redoubt volcano eruption on GE CF6-80C2 turbofan engines, In Volcanic ash and aviation safety: Proc. of the First International Symposium on Volcanic Ash and Aviation Safety, US. Geological Survey Bulletin 2047, 129–135, Seattle, Washington, July, 1991, 1994.

Pujadas, M., Plaza, J., Teres, J., Artinano, B., Millan, M. (2000). Passive remote sensing of nitrogen dioxide as a tool for tracking air pollution in urban areas: the Madrid urban plume, a case of study. Atmospheric Environment 34(19): 3041-3056.

Salvador, P., Artinano, B., Alonso, D. G., Querol, X., Alastuey, A. (2004). Identification and characterisation of sources of PM10 in Madrid (Spain) by statistical methods. Atmospheric Environment 38(3): 435-447.

Schwab, J. J., Hogrefe, O., Demerjian, K. L., Dutkiewicz, V. A., Husain, L., Rattigan, O. V., Felton, H. D. (2006). Field and laboratory evaluation of the Thermo Electron 5020 Sulfate Particulate Analyzer. Aerosol Science and Technology 40(10): 744-752.

Stohl, A., Forster, C., Frank, A., Seibert, P., Wotawa, G. (2005). Technical note: The Lagrangian particle dispersion model FLEXPART version 6.2. Atmospheric Chemistry and Physics 5: 2461-2474.

Stohl, A., G. Wotawa, P. Seibert, and H. Kromp-Kolb (1995): Interpolation errors in wind fields as a function of spatial and temporal resolution and their impact on different types of kinematic trajectories. J. Appl. Meteor. 34, 2149-2165.

Sturkell, Erik, Einarsson, Páll, Sigmundsson, Freysteinn, Hooper, Andy, Ófeigsson, Benedikt G., Geirsson, Halldór, Ólafsson, Halldór, Anders Schomacker, Johannes Krüger and Kurt H. Kjær. 2 Katla and Eyjafjallajökull Volcanoes. Developments in Quaternary Science, Elsevier. Volume 13: 5-21.

Wang, S. C. and R. C. Flagan (1990). Scanning Electrical Mobility Spectrometer. Aerosol Science and Technology 13(2): 230-240.

Figures

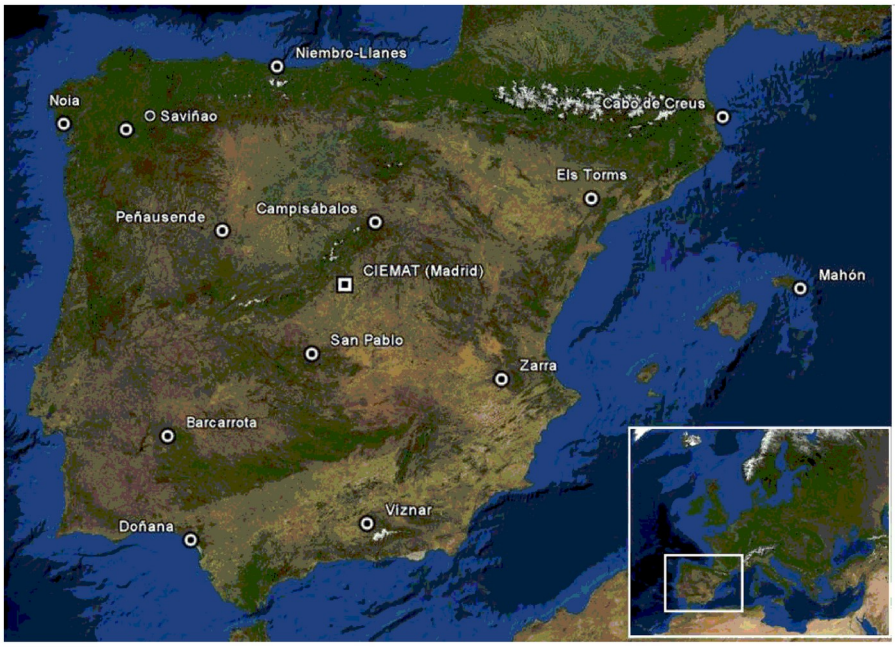

Figure 1. Geographical situation of the measurements sites, with the Spanish EMEP/GAW/CAMP stations represented by circles and the CIEMAT site (40.45ºN, 173.73ºW, 669 m asl) by a square. The coordinates of the EMEP/GAW/CAMP stations are shown in Table I.

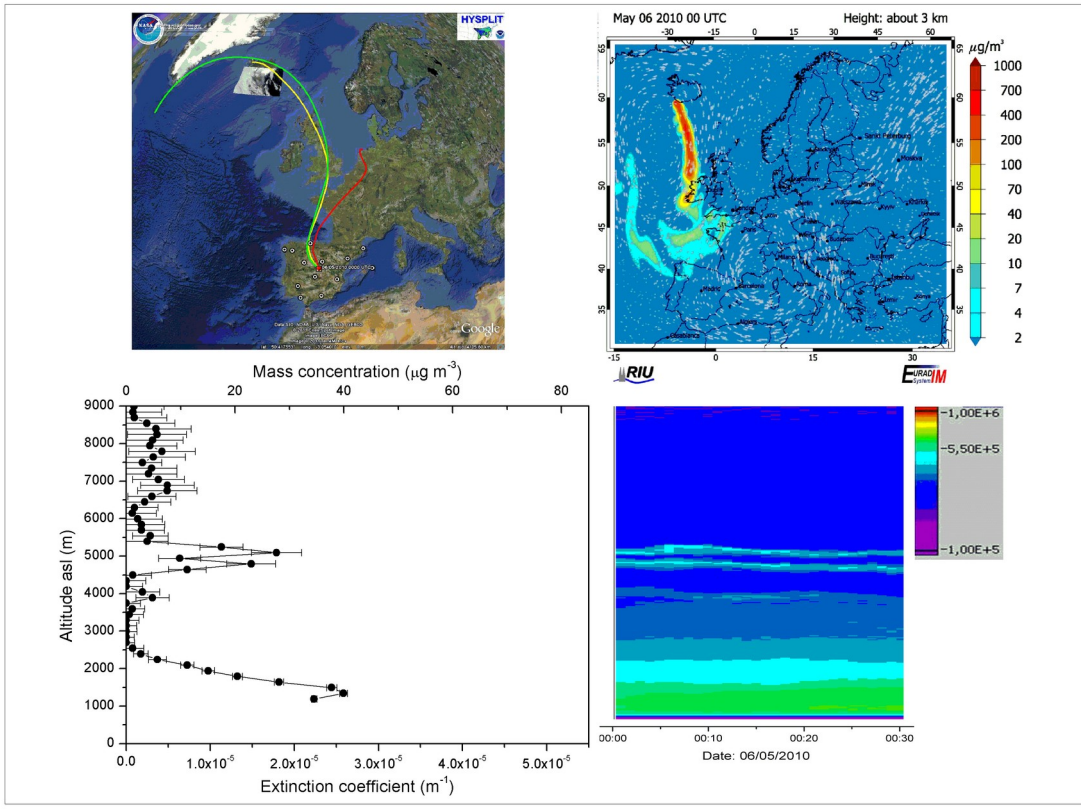

1**Figure 2**

2Characterization of the atmospheric situation over Madrid on 06/05/2010 00:00 UTC by 3means of 72-h backward trajectories provided by Hysplit model ending over Madrid at 42500 m (red), 5000 m (yellow) and 7500 m (green), (top left), 3-km height plume 5dispersion provided by EURAD model (top middle), extinction coefficient vertical profile 6provided by the Raman LIDAR (bottom left) and the quicklook produced as color-coded 7plots of the range-corrected LIDAR signals vs. time and height (bottom right).

8

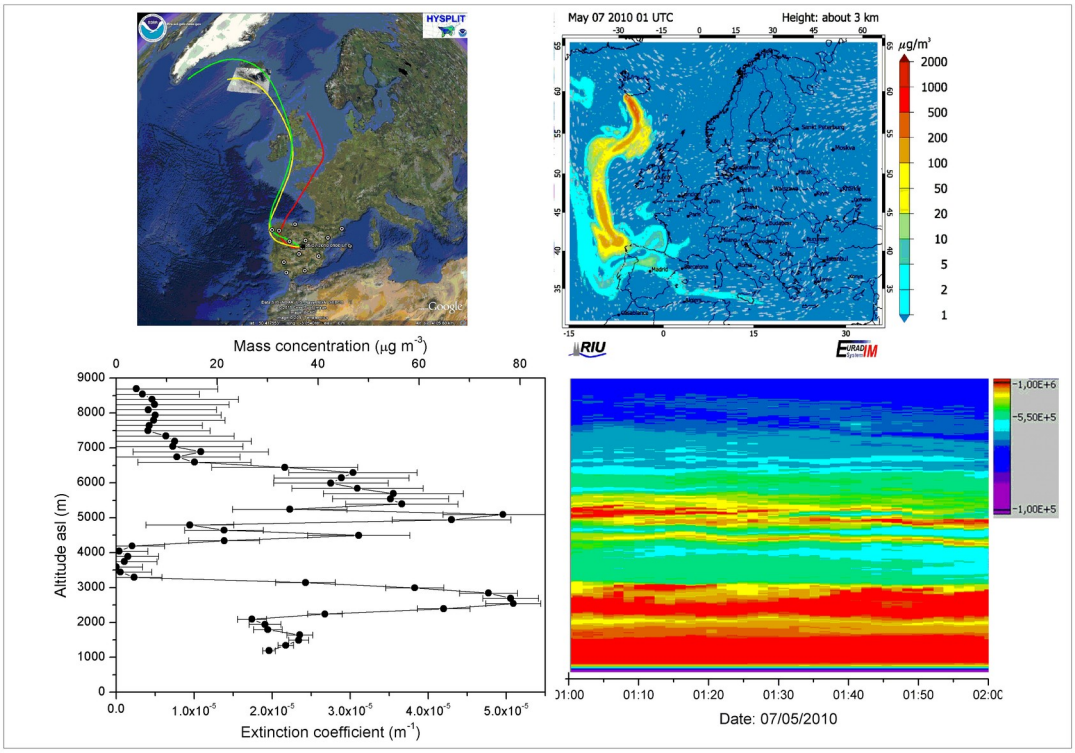

9**Figure 3**

10Same as figure 2, for 07/05/2010 01:00 UTC.

11

1

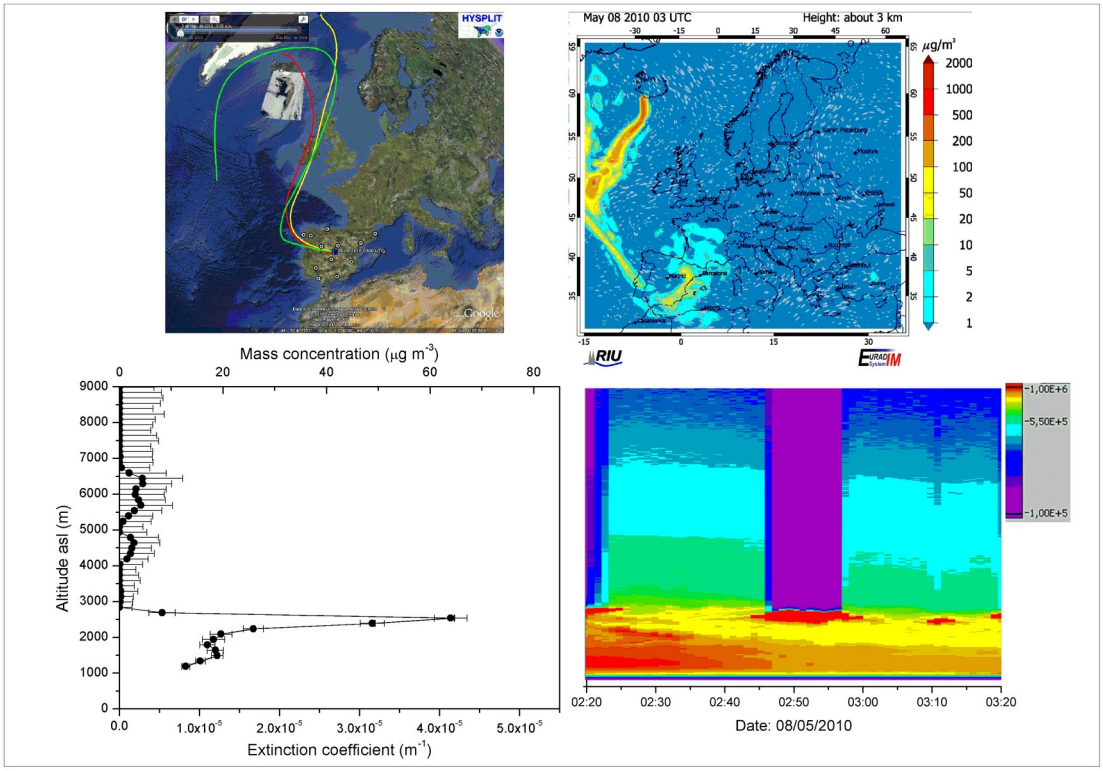

2**Figure 4**

3Same as figure 2, for 08/05/2010 02:00 UTC.

4

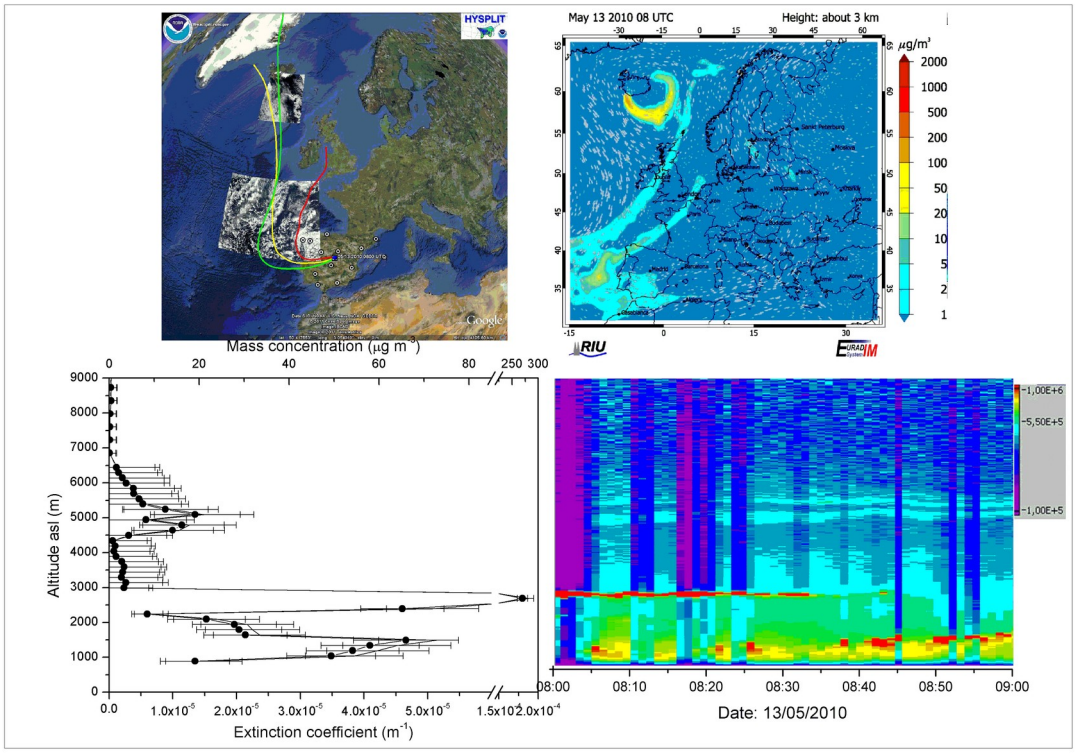

1**Figure 5**

2Same as figure 2, for 13/05/2010 08:00 UTC.

3

4

5

6

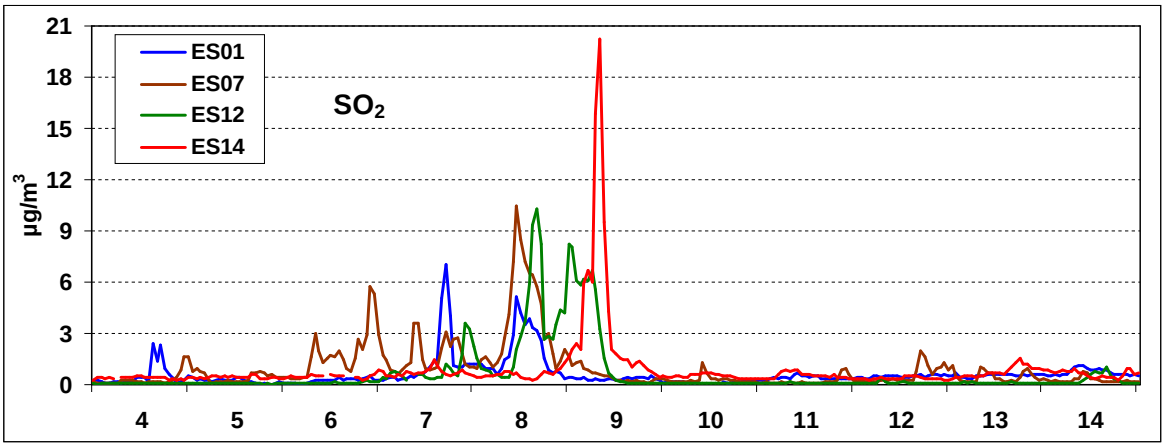

Figure 6

SO_2 concentration at San Pablo de los Montes (ES01), Víznar (ES07), Zarra(ES12) and Els Torms (ES14) between 4 and 14 May 2010.

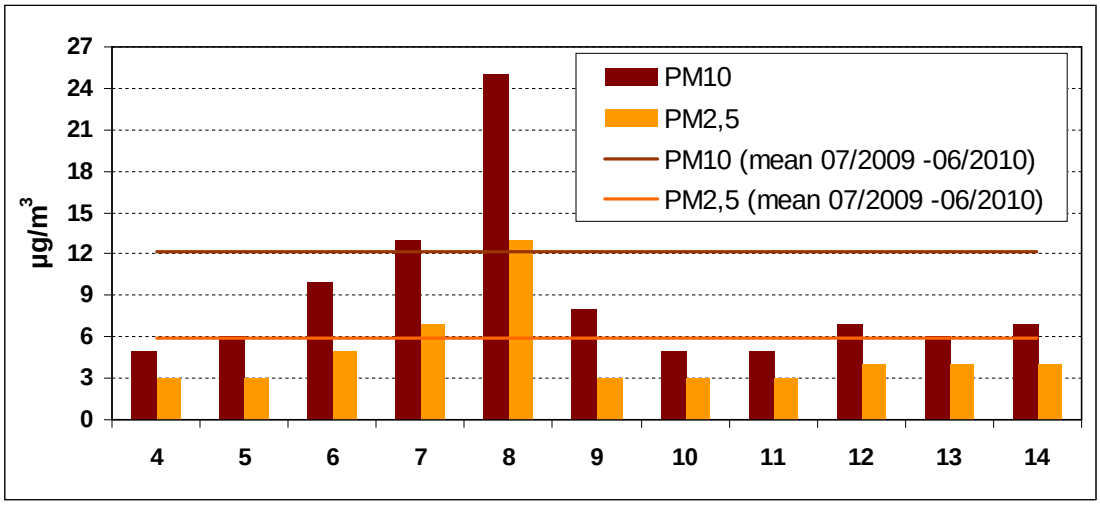
µg/m3
27
24
21
18
15
12
9
6
3
0
4
5
6
7
8
9
10
11
12
13
14
PM10
PM2,5
PM10 (mean 07/2009 -06/2010)
PM2,5 (mean 07/2009 -06/2010)

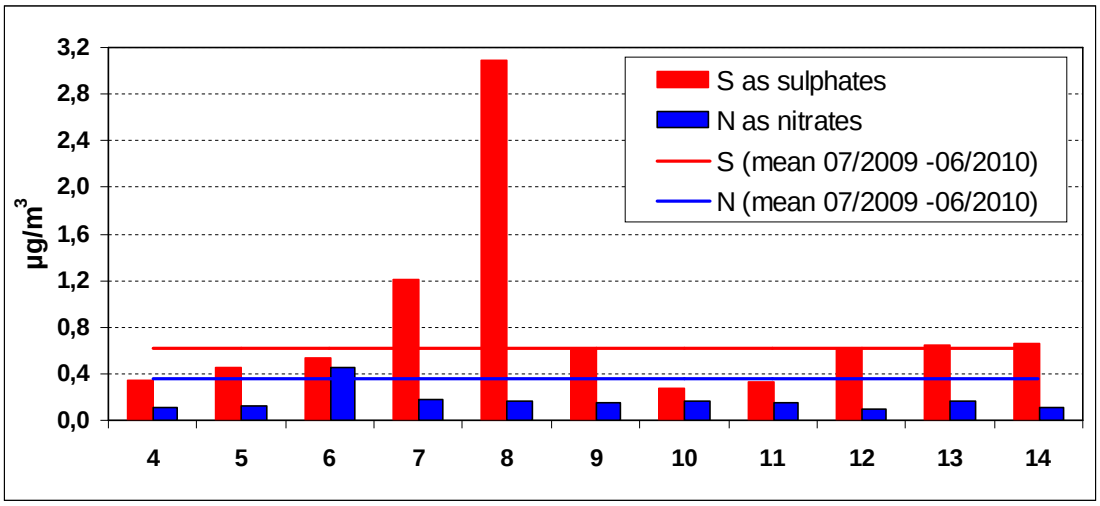
µg/m3
3,2
2,8
2,4
2,0
1,6
1,2
0,8
0,4
0,0
4
5
6
7
8
9
10
11
12
13
14
S as sulphates
N as nitrates
S (mean 07/2009 -06/2010)
N (mean 07/2009 -06/2010)

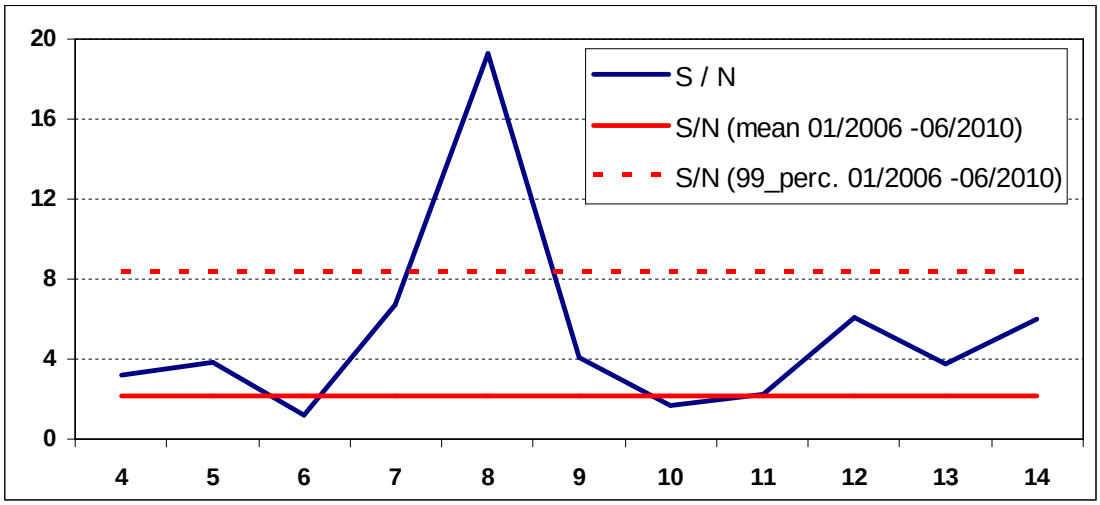
20
16
12
8
4
0
4
5
6
7
8
9
10
11
12
13
14
S / N
S/N (mean 01/2006 -06/2010)
S/N (99_perc. 01/2006 -06/2010)

2**Figure 7**

1(Top) PM_{10} and $PM_{2.5}$ concentrations at Zarra. The mean values are calculated from July 22009 to June 2010. (Middle) Sulfur as sulfates and nitrogen as nitrates concentrations in 3PM_{10} at Zarra. The mean values are calculated from July 2009 to June 2010. (Bottom) S/N 4ratio (where S is sulfur as sulfate and N is nitrogen as nitrate) obtained in PM_{10} at Zarra. 5The mean values are calculated from January 2006 to June 2010.

6

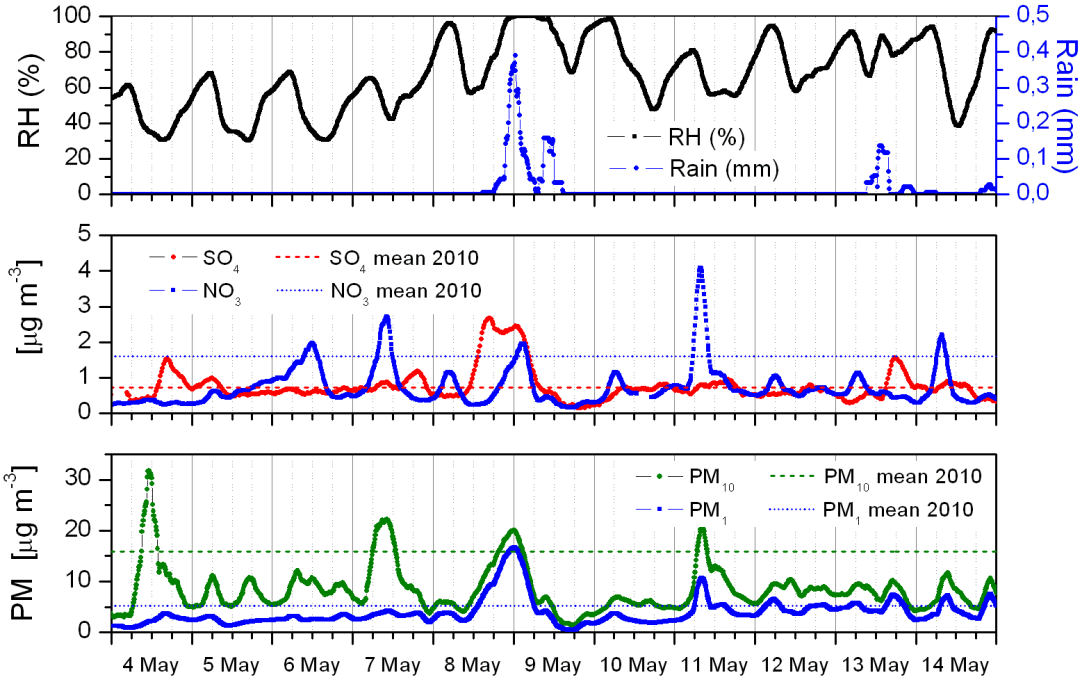

7**Figure 8**

8Temporal evolution of relative humidity and rain (top panel), PM_1 particulate sulfate and 9$PM_{2.5}$ nitrate concentration (central panel) and particle concentration (bottom panel) from 4 10to 14 May at CIEMAT.

11

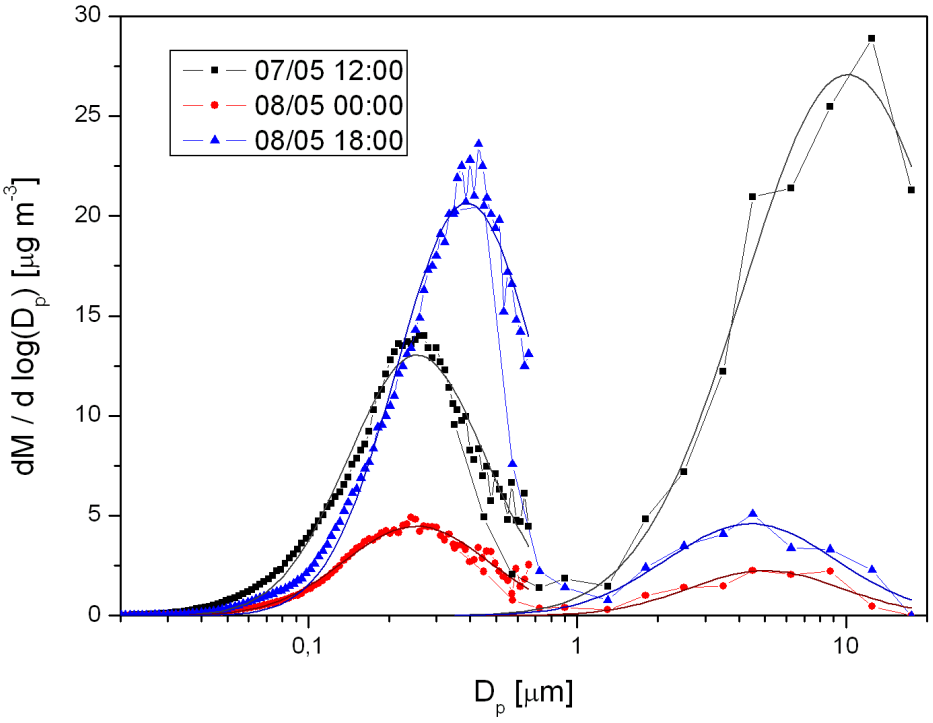

1**Figure 9**

23h-averaged mass distributions for the event of 7-9 May.

3

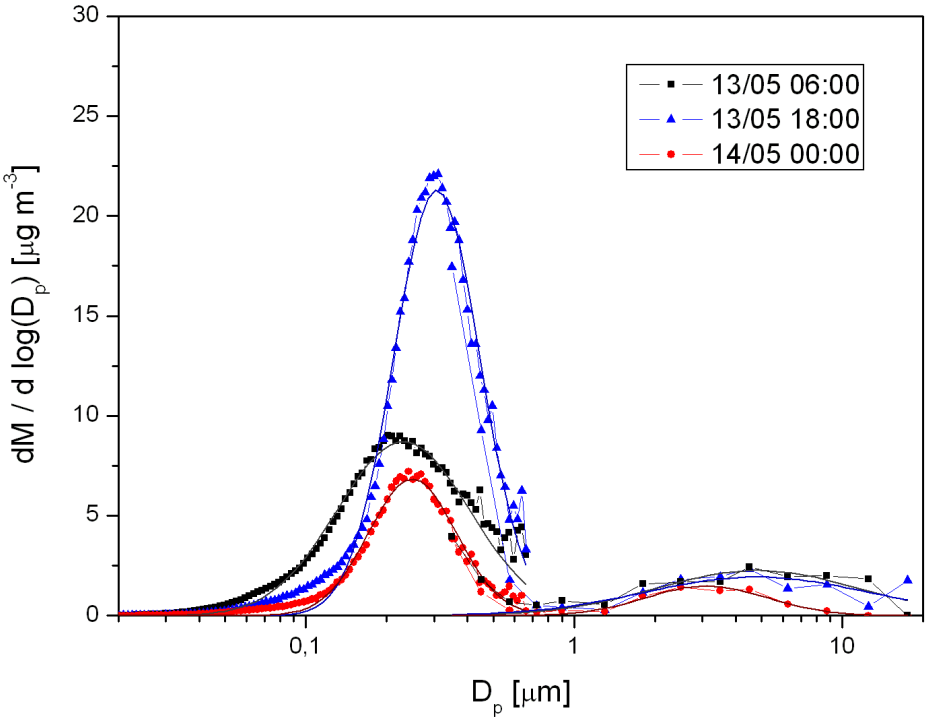

1**Figure 10**

23h-averaged mass distributions for the event of the 13-14 May.

3

4**Tables**

5

Code	*Station name and coordinates*	*SO_2*	*PM_{10}*	*$PM_{2.5}$*	*Precipitation*
ES01	San Pablo de los Montes (Toledo). 39.55º N, 4.35º W, 917 m asl.	THERMO 43CTL	ANDERSEN 236091	MCV-CAV	EIGENBRODT D 21225
ES05	Noia (A Coruña). 42,72º N, 8,92º W, 685 m asl.	THERMO 43CTL	TISCH T30 2X	********* *	EIGENBRODT NSA 181/S
ES06	Mahón (Menorca). 39,88º N, 4,32º E, 78 m asl.	THERMO 43CTL	TISCH TE-557	********* *	EIGENBRODT NSA 181/S
ES07	Víznar (Granada) 37,24º N, 3,53º W, 1.230 m asl.	THERMO 43BS	MCV	MCV	ERNI ARS 721
ES08	Niembro-Llanes (Asturias). 43,44º N, 4,85º W, 134 m asl.	THERMO 43BS	MCV	MCV	MCV CPH 004
ES09	Campisábalos (Guadalajara). 41,27º N, 3,14º W, 1.360 m asl.	THERMO 43BS	ANDERSEN GUV15H	DIGITEL DAH 80 A	MCV CPH 004
ES10	Cabo de Creus (Girona). 42,32º N, 3,31º E, 23 m asl.	THERMO 43BS	MCV	MCV	**********
ES11	Barcarrota (Badajoz). 38,47º N, 6,92º W, 393 m asl.	THERMO 43BS	MCV	MCV	MCV CLA 001
ES12	Zarra (Valencia). 39,08º N, 1,10º W, 885 m asl.	THERMO 43BS	MCV	MCV	MCV CPH 004
ES13	Peñausende (Zamora). 41,23º N, 5,89º W, 985 m asl.	THERMO 43BS	MCV	MCV	MCV CPH 001
ES14	Els Torms (Lleida). 41,39º N, 0,73º E, 470 m asl.	THERMO 43BS	MCV	MCV	MCV CPH 004
ES16	O Saviñao (Lugo). 42,63º N, 7,70º W, 506 m asl.	THERMO 43BS	MCV	MCV	ERNI ARS 721
ES17	Doñana (Huelva). 37,05º N, 6,56º W, 5 m asl.	THERMO 43CTL	ANDERSEN 2360	**********	EIGENBRODT NSA 181/S

1**Table I**

2Coordinates of the EMEP/GAW/CAMP stations and pollutant measurement technique.

3

4

Mode	Date	Time	d_g (μm)	σ_g(μm)	D_p (μm)
Fine	07/05/2010	12:00	0.359±0.005	1.802±0.015	0.254±0.004
	08/05/2010	00:00	0.370±0.006	1.859±0.018	0.252±0.005
	08/05/2010	18:00	0.556±0.011	1.816±0.019	0.390±0.009
	13/05/2010	06:00	0.358±0.005	1.871±0.017	0.242±0.004
	13/05/2010	18:00	0.353±0.002	1.450±0.007	0.307±0.002
	14/05/2010	00:00	0.287±0.002	1.458±0.007	0.249±0.002
Coarse	07/05/2010	12:00	22.4±4.6	2.44±0.19	10.1±2.5
	08/05/2010	00:00	7.8±1.2	1.94±0.19	5.0±1.0
	08/05/2010	18:00	7.5±1.0	2.07±0.15	4.4±0.7
	13/05/2010	06:00	10.3±3.1	2.39±0.37	4.8±2.0
	13/05/2010	18:00	12.1±6.8	2.62±0.70	4.8±3.7
	14/05/2010	00:00	4.1±0.2	1.68±0.07	3.1±0.2

1**Table II**

2Values obtained for the fitting of lognormal distribution to the fine mode, measured by the

3SMPS instrument, and coarse mode, measured by the GRIMM OPC.